

1 **Room temperature mid-infrared InAsSbN multi-quantum well photodiodes**  
2 **grown by MBE**

3  
4  
5  
6  
7  
8  
9  
10  
11  
12  
13  
14  
15  
16  
17  
18  
19  
20  
21  
22  
23  
24  
25  
26  
27  
28  
29  
30  
31  
32  
33  
34  
35  
36

M. Kesaria\*, M. de la Mare, A. Krier

*Physics Department, Lancaster University, Lancaster, LA1 4YB, UK*

\*Corresponding author email: [m.kesaria@lancaster.ac.uk](mailto:m.kesaria@lancaster.ac.uk)

**Key Words:** Dilute Nitride, InAsSbN, MBE, Photodiodes

1 **Abstract**

2  
3  
4  
5  
6  
7  
8  
9  
10  
11  
12  
13  
14  
15  
16  
17  
18  
19  
20  
21  
22  
23  
24  
25  
26  
27  
28  
29  
30  
31  
32  
33  
34

Room temperature photoresponse in the mid-infrared spectral region is demonstrated from InAsSbN/InAs multi-quantum well photodiodes grown by nitrogen plasma assisted molecular beam epitaxy. The structural quality of the InAsSbN MQWs was ascertained *in-situ* by reflection high energy electron diffraction and *ex-situ* by high resolution X-ray diffraction and photoluminescence measurements. The extended long wavelength photoresponse is identified to originate from the electron-heavy hole ( $e_1-hh_1$ ) and electron-light hole ( $e_1-lh_1$ ) transitions in the InAsSbN MQW, with a cut off wavelength  $\sim 4.20 \mu\text{m}$  and peak detectivity  $D^* = 1.25 \times 10^9 \text{ cm Hz}^{1/2} \text{ W}^{-1}$ .

1  
2  
3  
4  
5  
6  
7  
8  
9  
10  
11  
12  
13  
14  
15  
16  
17  
18  
19  
20  
21  
22  
23  
24  
25  
26  
27  
28  
29  
30  
31  
32  
33  
34

## Introduction

Photodetectors operating in the mid-infrared spectral range (3-5  $\mu\text{m}$ ) are of technological importance due to their military applications in infrared countermeasures and night vision as well as many civil applications, including atmospheric pollution monitoring, optical spectroscopy and medical diagnostics. Mercury cadmium telluride (MCT) photodetectors are commonly used for some of these applications together with InGaAs, InSb, InAsSb [1] and InAsSbP [2]. MCT alloys have a small electron effective mass ( $\sim 0.009 m_0$ ) resulting in undesirable dark currents due to tunnelling and require cooling. These alloys also suffer from compositional non-uniformity which compromises the detector spectral response over large areas [3-5]. Access to mid-infrared wavelengths can also be achieved using alternative III-V based material systems such as InAsN, where the addition of small amounts ( $< 1\%$ ) of nitrogen into InAs has been found to substantially reduce the band gap and allow tailoring of the detection wavelength [6-9]. Research into dilute nitride materials can give insight into fundamental physics and also has potential for the development of new high performance detectors and large-format focal plane arrays [10-11].

Room temperature electroluminescence (EL) at a peak wavelength  $\sim 3.7 \mu\text{m}$  was demonstrated earlier from type II InAsSb/InAs multi-quantum well (MQW) light-emitting diodes (LEDs) [12]. The introduction of nitrogen into InAsSb quantum wells changes the band alignment from type-II to type-I due to an increase in the electron confinement and bandgap reduction, with no excess strain. The surfactant effect of Sb during growth enhances the crystalline and optical quality of InAsSbN, whereas the adjustment of Sb and N contents enables lattice matching to InAs and strain tailoring in the QW. Previously, we have reported good quality InAsSbN alloys, InAsSbN p-i-n diodes emitting near  $4.0 \mu\text{m}$  at room temperature [13-15], InAsSbN MQW [16] and InAsSbN MQW LEDs emitting at  $3.6 \mu\text{m}$  (4 K) [17]. More recently InAsN and InGaAsN MQW implemented on InP substrate have been shown to enable dilute nitride mid-infrared laser diodes [18]. InAsSbN quantum wells [19] and laser diodes [20] have also been reported elsewhere in the literature, but there are very few studies on dilute nitride photo-detectors operating in the 2-5  $\mu\text{m}$  spectral range [21-23].

In this work, we demonstrate InAsSbN MQW photodiodes grown on InAs substrate by plasma assisted molecular beam epitaxy. The structural quality of the InAsSbN MQWs was ascertained by high resolution X-ray diffraction and photoluminescence measurements. Room temperature photoresponse was observed in the mid-infrared, with a cut-off wavelength near  $4.20 \mu\text{m}$  and a peak detectivity of  $D^* = 1.25 \times 10^9 \text{ cm Hz}^{1/2} \text{ W}^{-1}$ . The extended long

1 wavelength response was identified to originate from confined states of the dilute nitride  
2 MQW ( $e_1$ - $hh_1$  and  $e_1$ - $lh_1$ ) which is in good agreement with calculated values.

3

#### 4 **Experiment**

5

6 A VG-V80H molecular beam epitaxy (MBE) reactor was used to grow the InAsSbN quantum  
7 wells on n-InAs (001) substrates, as well as the complete MQW photodiode device structure.  
8 During growth *in-situ* characterization was performed by reflection high energy electron  
9 diffraction (RHEED). In, Al and Ga fluxes were provided by Knudsen thermal effusion cells.  
10 The  $As_2$  and  $Sb_2$  was generated from valved cracker cells and the atomic N flux by a Veeco  
11 Uni-bulb radio frequency plasma nitrogen source. The nitrogen flux was generated using a  
12 load power of 210 W and a nitrogen beam equivalent pressure (BEP)  $\sim 7.0 \times 10^{-7}$  mbar. BEP  
13 ratio of As/Sb = 2.6 and As/N = 3.7 (BEP of Sb  $\sim 1.1 \times 10^{-6}$  mbar, BEP of  $N_2$   $\sim 7.0 \times 10^{-7}$   
14 mbar and As  $\sim 2.6 \times 10^{-6}$  mbar). To optimize N incorporation into the MQW the minimum  
15 As flux was used during the growth of the InAs layers, since the adatom sites are more  
16 favourable for As than for N incorporation. In order to ascertain surface cleanliness and  
17 monitor crystalline quality, surface reconstructions were monitored by RHEED. Typical ( $2 \times$   
18  $4$ ) and ( $1 \times 3$ ) RHEED patterns shown in Figure 1a were observed during the growth in [011]  
19 and [0-11] directions for the InAs and InAsSbN surfaces, respectively. The substrate  
20 temperature was measured using an infrared pyrometer and back-calibrated by monitoring  
21 surface reconstruction transitions at a fixed As flux. The substrate preparation and oxide  
22 desorption was carried out in the conventional manner in the growth chamber. To desorb  
23 oxide from the InAs substrate required heating gradually up to 520 °C under As flux, (until a  
24 weak  $\times 3$  RHEED pattern transformed to the brighter  $\times 2$  pattern) [24]. To obtain abrupt  
25 quantum well interfaces and realize a low residual carrier concentration  $\sim 2 \times 10^{17}$  cm<sup>-3</sup> in the  
26 MQW, the surface was exposed to Sb for 3s (Sb flux  $\sim 3 \times 10^{-7}$ ) prior to InAsSbN quantum  
27 well growth and before the InAs barrier growth the surface was exposed to As (flux  $\sim 4 \times 10^{-6}$   
28 mbar) for 20 sec . The RHEED pattern was clearly  $1 \times 3$  at the beginning of the active region  
29 and transformed to  $2 \times 4$  under  $As_2$  flux, suggesting an efficient As–Sb exchange reaction  
30 and excess Sb removal from the surface. The structural quality and material composition was  
31 determined using high resolution x-ray diffraction (HRXRD) measurements. The resulting  
32 wafers were processed into 1 mm diameter mesa-etched diodes using standard  
33 photolithographic and wet etching techniques before mounting onto TO-46 headers.  
34 Photoluminescence (PL) and electroluminescence (EL) measurements were performed using

1 an Oxford Instruments variable temperature continuous flow He cryostat. The emitted  
2 radiation was collected using  $\text{CaF}_2$  lenses and focused into a 0.3m Bentham M300 grating  
3 monochromator. For EL the devices were tested at 1 kHz using a 50 % duty cycle excitation  
4 and the radiation was detected using a cooled (77 K) InSb photodiode detector and a Stanford  
5 Research (SR850) digital lock-in amplifier. The photo-response was measured using an Oriel  
6 Instruments 80007 silicon carbide source with a 1200 K colour temperature that was chopped  
7 at 175 Hz.

8 A schematic representation of the MQW structure and the corresponding photodiode detector  
9 is shown in Figures 1(b) and (c), respectively. The MQW structure consists of ten  
10  $\text{InAs}_{0.942}\text{Sb}_{0.050}\text{N}_{0.008}$  quantum wells, each 10 nm wide with 25 nm InAs barriers, grown on  
11 InAs substrate. For the photodiode a 0.5  $\mu\text{m}$  Te doped InAs layer is grown on InAs at 490 °C  
12 (1  $\mu\text{m}/\text{h}$  growth rate) which is followed by ten 10 nm  $\text{InAs}_{0.942}\text{Sb}_{0.050}\text{N}_{0.008}$  quantum wells  
13 with 25nm InAs barriers (0.5  $\mu\text{m}/\text{h}$  growth rate) at lower substrate temperature 410 °C. The  
14 growth temperature is raised to 490 °C for the growth of the 30 nm undoped  
15  $\text{Al}_{0.90}\text{Ga}_{0.10}\text{As}_{0.21}\text{Sb}_{0.79}$  electron blocking barrier above the active region and finally capped by  
16 500 nm thick Be-doped InAs.

17

## 18 **Results and discussion**

19

20 The incorporation of N or Sb into InAs layers is known to introduce tensile or compressive  
21 strain respectively. Therefore, addition of 0.8% N to  $\text{InAs}_{0.95}\text{Sb}_{0.05}$  MQW reduces  
22 compressive strain from 0.5% to 0.2% allowing strain-balancing and we used this in the  
23 growth of the InAsSbN MQW structure and photodiode used here. The corresponding  
24 HRXRD rocking curves are shown in Figure 2 (a) and (b), respectively. The peak at 858 arc  
25 seconds corresponds to the  $\text{Al}_{0.90}\text{Ga}_{0.10}\text{As}_{0.21}\text{Sb}_{0.79}$  layer in the photodiode. The diffraction  
26 pattern of both structures has a distinct zero order peak and a few high-order satellite peaks.  
27 The absence of higher angle satellite peaks can be due to atomic level roughness at the  
28 interface between the well and barrier. In our earlier work we have shown that in  
29 InAsSbN/InAs MQWs the interface between the well and barrier can have roughness up to  $\pm$   
30 2 nm [17]. InAsSbN epilayers (1 $\mu\text{m}$  thick) grown on InAs substrate in different Sb and N  
31 conditions were used to determine Sb and N composition [14-16]. Simulation of the  
32 structures was done using Bede RADS software which is based on the dynamical scattering  
33 theory of diffraction. The solid lines (black) are experimental results and the dashed lines

1 (blue) are simulated data. The derived thicknesses of the perfectly strain balanced InAsSbN  
2 well and InAs barrier are approximately 10 nm and 25 nm, respectively.

3

4 Figure 3 shows (a) the 4 K PL emission spectrum and (b) the 300 K EL spectrum. The  
5 experimental PL and EL data were de-convoluted by fitting Gaussian peaks. For the 4 K PL  
6 these peaks are centred at 0.340 and 0.355 eV, which is approximately in agreement with the  
7 calculated  $e_1$ - $hh_1$  and  $e_1$ - $lh_1$  QW transitions, respectively. The calculation of the transition  
8 energies was done using a Schrodinger solver within an effective mass approximation, taking  
9 into account N-induced band anti-crossing effects, coupling constants and strain [16]. The  
10 difference between calculated and experimental values originates from uncertainties in N and  
11 Sb content and also the effective masses within the QW [25]. The room temperature EL  
12 spectrum shown in Fig 3(b) was similarly de-convoluted into three peaks which are centred at  
13 0.318 eV, 0.349 eV and 0.396 eV, respectively. The first being attributed to  $e_1$ - $hh_1$  QW  
14 transition, while the peaks at 0.349 eV and 0.396 eV arises from recombination taking place  
15 in the intrinsic  $n^0$  InAs barriers and  $n^+$  InAs, respectively.

16 Figure 4 compares the room temperature photoresponse of (a) an InAs photodiode (with an  
17 InAsSbP window) [26], (b) the InAsSbN MQW photodiode, and (c) the electroluminescence  
18 from the InAsSbN MQW diode. The photoresponse of the InAsSbN MQW photodiode  
19 extends from 1.10 to 4.20  $\mu\text{m}$  having an extended cut off at 4.20  $\mu\text{m}$  compared with the cut  
20 off wavelength for InAs at 3.88  $\mu\text{m}$ . The maximum of the electroluminescence spectrum at  
21 3.57  $\mu\text{m}$  is 0.63  $\mu\text{m}$  lower than the cut-off of the MQW diode photoresponse.

22 Current-voltage (I-V) curves were obtained at temperatures 20 K to 300 K for the InAsSbN  
23 MQW photodiode. Figure 5 (a) shows a semi-logarithmic plot of the I-V curves acquired at  
24 20, 160 and 300 K using a bias in the range -0.4 to 0.8 V from which the corresponding diode  
25 series resistance is estimated as  $\sim 2.5 \Omega$  and the ideality factor ( $\beta$ )  $\sim 1.56$  below 150 K. The  
26 diode reverse leakage current decreased from 2 mA to 0.7 mA with a reduction in  
27 temperature from 300 K to 20 K. To understand the current conduction mechanisms an  
28 Arrhenius plot of zero bias resistance area ( $R_0A$ ) was extracted and is shown in Figure 5(b).  
29 The  $R_0A$  values grow exponentially with decreasing temperature, but the growth rate is  
30 different at high and low temperatures. The straight lines show the fits obtained using the  
31 energy ( $E = 0.29$  eV) in the exponent ( $\exp E/\beta kT$ ) which is close to the  $e_1$ - $hh_1$  transition of  
32 the InAsSbN (N $\sim$ 1%) MQWs. The results are consistent with diffusion current ( $\beta\sim 1$ ) in the  
33 200-300 K temperature range. At low temperatures generation recombination current

1 dominates consistent with  $\beta \sim 2$ . The specific (peak) detectivity of the InAsSbN MQW  
2 photodiode was determined as  $D^* = 1.25 \times 10^9 \text{ cm Hz}^{1/2} \text{ W}^{-1}$  at 300 K for the mesa etched  
3 1mm diameter diodes in this work, using the Johnson noise limited equation [27]. This is  
4 comparable with previously reported InAsSb (InAsSbP) photodiodes at 300K<sup>1-2</sup> and is  
5 encouraging since the MQW diodes are not yet optimized or anti-reflection coated. The  
6 valence band offsets (62 meV) of the MQWs are small enough to allow the photogenerated  
7 carriers to escape at 300 K and the number of QW can be increased further to increase  
8 absorption using strain balancing. Consequently, this material system shows promise as the  
9 addition of N provides an additional freedom in tailoring the band structure within a type I  
10 QW system at longer wavelengths. To improve device quality, further work is in progress to  
11 reduce the active region residual carrier concentration and improve the MQW interface  
12 quality as well as extend the wavelength range by introduction of more nitrogen.

13

## 14 **Conclusions**

15

16 We have demonstrated uncooled InAsSbN/InAs MQW photodiodes, grown strain balanced  
17 on InAs by MBE, which exhibit a photoresponse in the mid-infrared spectral range at 300 K.  
18 The structural and optical quality were ascertained by high resolution X-ray diffraction and  
19 photo-/electroluminescence. The diodes exhibit responsivity in the mid infrared spectral  
20 region with an extended long wavelength response, which is identified to originate from the  
21 InAsSbN e-hh<sub>1</sub> and e-lh<sub>1</sub> transitions and is in agreement with calculated values. The  
22 photodiodes exhibit a cut-off wavelength of near 4.2  $\mu\text{m}$  at room temperature with a specific  
23 detectivity,  $D^* = 1.25 \times 10^9 \text{ cm Hz}^{1/2} \text{ W}^{-1}$  at 300 K. Since InAsSbN enables strain-balancing  
24 on InAs the dilute nitride alloys offer some additional freedom in tailoring long wavelength  
25 photodetectors.

26

## 27 **Acknowledgements**

28 The authors are grateful to the Engineering and Physical Science Research Council (EPSRC)  
29 for financial support (grant EP/J015849/1).

30

31

32

33

34

## 1 References

- 2 [1] Gao H H, Krier A and Sherstnev V V 2000 Appl. Phys. Lett. **77**, 872.  
3 [2] Krier A and Suleiman W 2006 Appl. Phys. Lett. **89**, 083512.  
4 [3] Rogalski A 2005 Reports on Progress in Physics **68**, 2267.  
5 [4] Rogalski A 2012 Opto-Electronics Review **20**, 279.  
6 [5] Rogalski A 2010 Opto-Electronics Review **18**, 478.  
7 [6] Nishikawa A, Katayama R, Onabe K and Shiraki Y 2003 Journal of Crystal Growth  
8 **251**, 427.  
9 [7] [Ding-Kang S, Hao-Hsiung L, Li-Wei S, Tso-Yu C, Yang T R 2003, Japanese Journal](#)  
10 [of Applied Physics 42, 375.](#)  
11 [8] Bi W G and Tu C W 1997 Applied Physics Letters **70**, 1608.  
12 [9] Chang A S, Zech E S, Kim T W, Lin Y H, Mawst L J and Goldman R S 2014 Applied  
13 Physics Letters **105**, 142105.  
14 [10] Veal T D, Piper L F J, Jefferson P H, Mahboob I, McConville C F, Merrick M, Hosea  
15 T J C, Murdin B N, and Hopkinson M 2005 Applied Physics Letters **87**, 182114.  
16 [11] Kuroda M, Katayama R, Nishio S, Onabe K and Shiraki Y 2003 physica status solidi  
17 (c) **0**, 2765.  
18 [12] Krier A, Stone M, Zhuang Q D, Liu P-W, Tsai G and Lin H H 2006 Applied Physics  
19 Letters **89**, 091110.  
20 [13] Zhuang Q, Godenir A, Krier A, Tsai G and Lin H H 2008 Applied Physics Letters **93**,  
21 121903.  
22 [14] [Latkowska M, Baranowski M, Linhart WM, Janiaka F, Misiewicz J, Segercrantz N, et](#)  
23 [al. 2016 Journal of Physics D: Applied Physics 49, 115105.](#)  
24 [15] [Godenir A. Novel dilute nitride semiconductor materials for mid-infrared](#)  
25 [applications. PhD \[dissertation\]. Lancaster: Lancaster University; 2008. Available](#)  
26 [from: Lancaster E-prints](#)  
27 [16] [Martin de la M, Carrington P J, Wheatley R, Zhuang Q, Beanland R, Sanchez A M](#)  
28 [and A. Krier 2010 Journal of Physics D: Applied Physics 43, 345103.](#)  
29 [17] Carrington P J, de la Mare M, Cheetham KJ, Zhuang Q, Krier A 2011 Advances in  
30 OptoElectronics **2011**.  
31 [18] Wheatley R, Kesaria M, Mawst L J, Kirch J D, Kuech T F, Marshall A, Zhuang Q D  
32 and Krier A 2015 Applied Physics Letters **106**, 232105 (2015).  
33 [19] Shono T, Mizuta S and Kawamura Y 2013 Journal of Crystal Growth **378**, 69.  
34 [20] Kawamura Y and Inoue N 2007 Journal of Crystal Growth **301–302**, 963.  
35 [21] Tan K H, Yoon S F, Loke W K, Wicaksono S, Lew K L, Stöhr A, Ecin O, Poloczek  
36 A, Malcoci A and Jäger D 2007 Applied Physics Letters **90**, 183515.  
37 [22] Luna E, Hopkinson M, Ulloa J M, Guzmán A and Muñoz E 2003 Applied Physics  
38 Letters **83**, 3111.  
39 [23] Aina L, Hier H, Fathimulla A, Lecates M, Kolodzey J, Goossen K, Coppinger M and  
40 Bhargava N 2009 Infrared Physics & Technology **52**, 310.  
41 [24] [Bhatnagar K, Rojas-Ramirez J, Caro M, Contreras R, Henninger B, Droopad R. 2015](#)  
42 [Journal of Crystal Growth. 425, 16.](#)  
43 [25] Patanè A, Feu W H M, Makarovskiy O, Drachenko O, Eaves L, Krier A, Zhuang Q D,  
44 Helm M, Goiran M and Hill G 2009 Physical Review B **80**, 115207.  
45 [26] Krier A, Yin M, Marshall A R J, Kesaria M, Krier S E, McDougall S, Meredith W,  
46 Johnson A D, Inskip J and Scholes A 2015 Infrared Physics & Technology **73**, 126.  
47 [27] Dennis P N J 1986, Photodetectors (Plenum, New York, 1986).

48  
49  
50



1 **Figures with captions:**

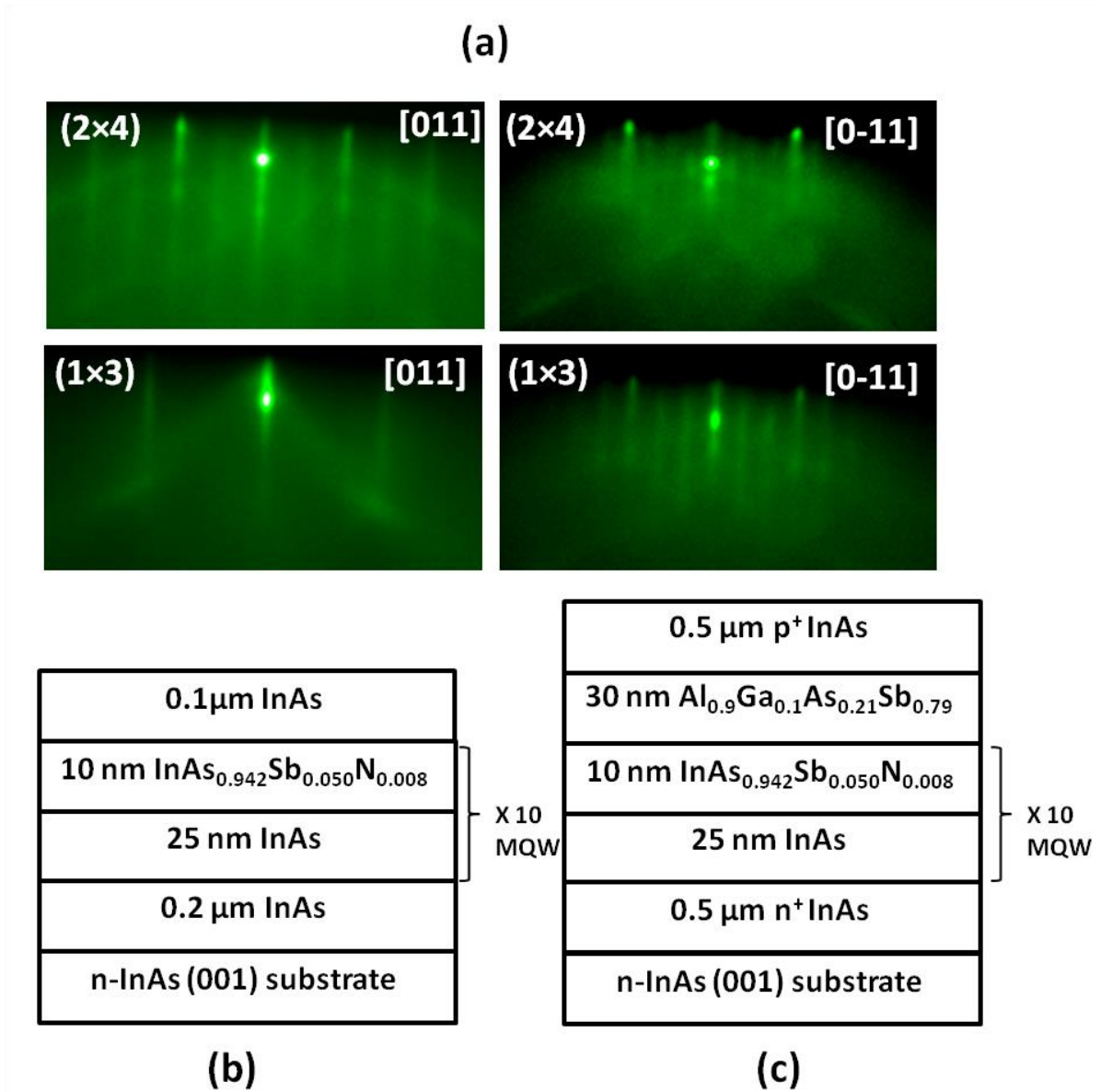
2

3 Figure 1

4

5

6



7

8

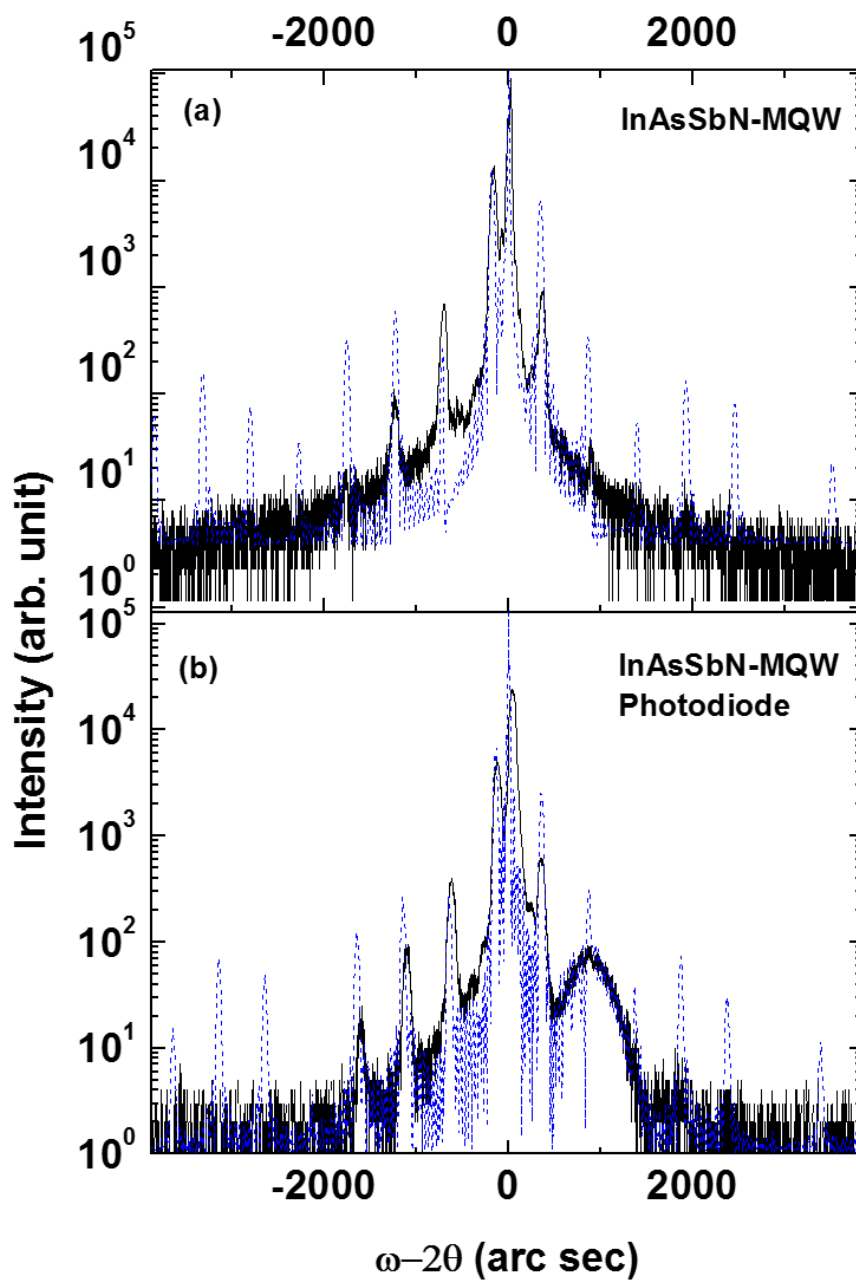
9 Figure 1. (a) typical  $2 \times 4$  and  $1 \times 3$  RHEED patterns for InAs and InAsSbN surface observed  
10 during the growth in the [011] and the [0-11] direction; (b) schematic details of the MQW  
11 structure used in the photodiode active region and (c) the complete photodiode structure, each  
12 containing 10 InAsSbN quantum wells.

13

14

1 Figure 2

2



3

4

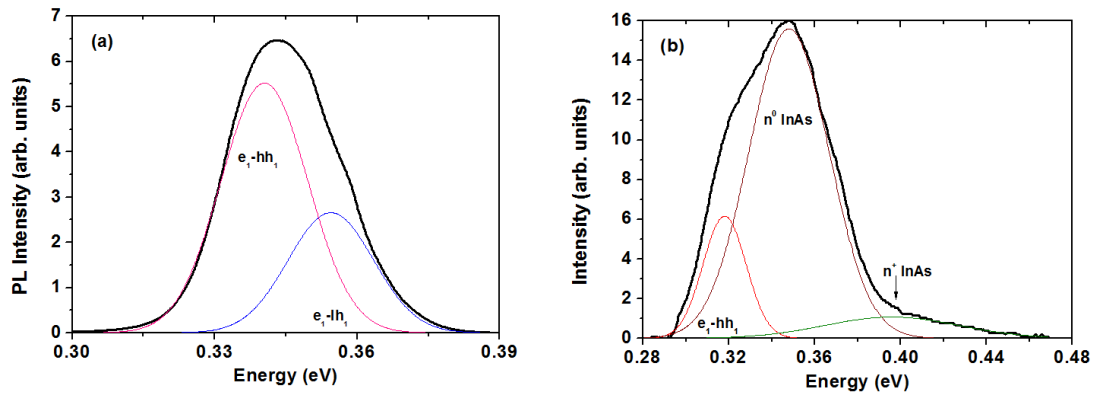
5 Figure 2 High resolution x-ray diffraction rocking curves (black) and simulated XRD patterns  
6 (blue dotted) of (a) the MQW active region and (b) the complete photodiode structure.

7

8

9

1 Figure 3



2

3

4 Figure 3 shows (a) the 4 K PL spectra and (b) 300K EL spectra in black - along with a close

5 fit envelope in red to the experimental data. The de-convoluted Gaussian peaks;  $e_1-hh_1$

6 (red),  $e_1-lh_1$  (blue),  $n^0$  InAs (brown) and  $n^+$  InAs (green) are labelled accordingly.

7

8

9

10

11

12

13

14

15

16

17

18

19

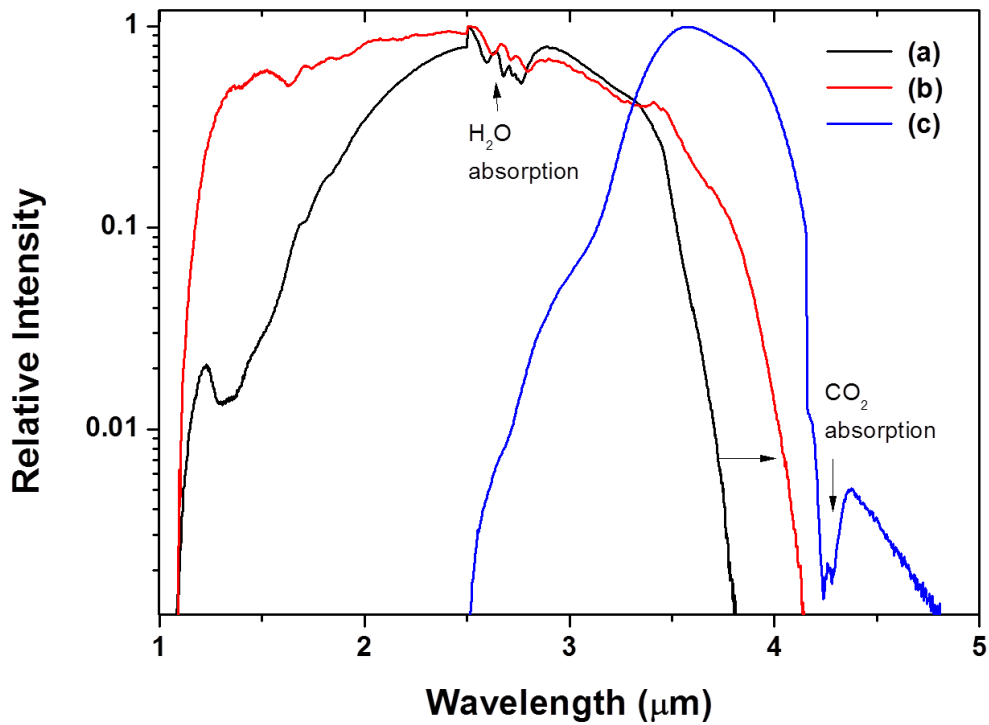
20

21

22

23

1 Figure 4

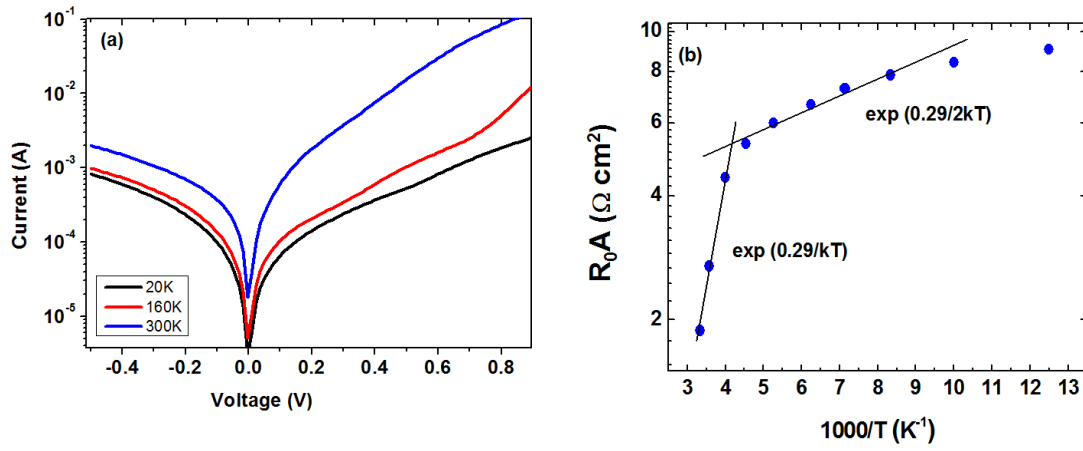


2  
3  
4  
5  
6  
7  
8  
9  
10  
11  
12  
13  
14  
15  
16  
17  
18

Figure 4 shows the room temperature logarithmic plots of (a) photoresponse from a bulk InAs photodiode with an InAsSbP window, (b) the InAsSbN MQW photodiode and (c) electroluminescence from the InAsSbN MQW diode (at injection current 100 mA). The photoresponse spectra both contain features due to atmospheric absorption from water vapour in the optical path around 2.7 μm.

1 Figure 5

2



3

4

5

6

7 Figure 5, (a) The I-V curves acquired at 20 K, 160 K and 300 K from the InAsSbN MQW

8 photodiode (data for other temperatures omitted for clarity); and (b) the zero bias resistance

9 area ( $R_0A$ ) versus reciprocal of temperature plot derived from the I-V measurements for the

10 same InAsSbN diode. The straight lines correspond to  $\exp (0.29/kT)$  and  $\exp (0.29/2kT)$ .

11